



HAL
open science

ISOGEOMETRIC ANALYSIS OF SPACE RODS: CONSIDERATIONS ON STRESS LOCKING

Massimo Cuomo, Leopoldo Greco

► **To cite this version:**

Massimo Cuomo, Leopoldo Greco. ISOGEOMETRIC ANALYSIS OF SPACE RODS: CONSIDERATIONS ON STRESS LOCKING. 2012. hal-00877888

HAL Id: hal-00877888

<https://hal.science/hal-00877888>

Submitted on 29 Oct 2013

HAL is a multi-disciplinary open access archive for the deposit and dissemination of scientific research documents, whether they are published or not. The documents may come from teaching and research institutions in France or abroad, or from public or private research centers.

L'archive ouverte pluridisciplinaire **HAL**, est destinée au dépôt et à la diffusion de documents scientifiques de niveau recherche, publiés ou non, émanant des établissements d'enseignement et de recherche français ou étrangers, des laboratoires publics ou privés.

ISOGOMETRIC ANALYSIS OF SPACE RODS: CONSIDERATIONS ON STRESS LOCKING

Massimo Cuomo¹ and Leopoldo Greco¹

¹University of Catania, Dept. of Civil and Environmental Engineering
viale A. Doria, 6 - 95125 Catania (Italy)
e-mail: mcuomo@dica.unict.it

Keywords: b-splines, space rods, multipatch analysis

Abstract. *The paper deals with the isogeometric analysis via B-splines of space rods under Kirchhoff-Love hypotheses. The approach has been used for developing space curve element within the framework of the Timoshenko rod model by many authors.*

In this work we develop a multi-patch isogeometric approach for the numeric analysis of the 3D Kirchhoff-Love rod theory. We use Bezier and B-splines interpolations and we show that they are able to attain very good accuracy for rod structures, particularly for developing a 3D exact curve element with geometric torsion. The patches in general present a C_n -continuity in the interior and are joined with C_0 -continuity, so that the global tangent stiffness operator in general is singular. In order to avoid the singularity in the stiffness operator several continuity conditions at the joints of the patches are required. Either parametric continuity (C_2 or C_3) or geometric continuity (G_1 or G_2) conditions can be imposed.

The geometric continuity conditions are weaker than the parametric conditions. The continuity conditions in the CAD -literature are known as the beta-constraints and represent constraint conditions for the displacements of the control points where the scalar beta-quantity represents additional unknowns. In this work, we don't impose the continuity conditions via beta-constraints but directly by means of the Lagrange's multipliers method.

1 INTRODUCTION

Structural models for curved space rods Model have been given by [1], [2], [3], in the context of Kirchhoff-Love hypotheses, and by [4], [5], for the Timoshenko model. In the context of standard polynomial interpolations many elements have been proposed for effectively treating this kind of structures, generally based on mixed or enhanced formulations [4],[5]. More recently, formulations that employ piecewise continuous interpolations on the elements have been proposed; the interelement continuity is imposed in a weak sense using the Discontinuous Galerkin approach [6].

Recently isogeometric analysis has been applied to many problems of solid and fluid mechanics. In isogeometric analysis C^{p-1} continuity is guaranteed, as opposite to the usual C^0 continuity obtained with the standard FEM discrete representations. Thanks to the high continuity properties, B-splines are very useful for beams and shells, since they can incorporate in the analysis the initial geometric curvatures without discontinuities. The patches in general present C^{p-1} continuity in the interior and are joined with C^0 continuity, in multi-patch models, so that the global tangent stiffness operator in general is singular. In order to avoid the singularity in the stiffness operator several strategies for imposing the continuity conditions at the joints of the patches have been described by many authors.

In the field of 1D structural theories rod models have been developed on the basis of the theory of Simo [7]. References [8], [9] are relative to polar beams, in [9] is interesting the idea to formulate a free-shear looking element via the collocation procedure of the discrete shear gaps for the isogeometric case. Timoshenko rod models are more common than Kirchhoff-Love model for finite deformation space rods, (since the continuity conditions for rotations are automatically imposed within a C^0 continuity). However, the Kirchhoff-Love model has the advantage of avoiding locking phenomena that are critical for slender elements. In a recent paper [10] a pure displacement finite deformation *B-Spline* isoparametric formulation of a space rod model based on the Kirchhoff-Love model has been proposed. Recently, in [11] the authors have been developed a C^1 -continuous finite element based on Hermitian shape functions for the plane case and successively in [12] for the more 3D general case.

In the paper it is introduced an implicit G^1 Kirchhoff-Love rod element for the analysis of the multi-patch assembly of space rods, in the case of open B-splines interpolations, see [13]. Although in general a single patch can be used for modeling a rod, and degrees of freedom can be added increasing the number of internal knots, there are cases when it is necessary to discretise the beam with more than one patch; important examples are reticulated and framed structures, composed by rods that are connected at the ends by rigid links requiring that the tangents keep their relative orientation during the deformation.

2 SPACE ROD MODEL

For slender rods the use of Kirchhoff-Lovemodel has some advantages over the shear deformation Timoshenko model. It carries about a reduction in the number of degrees of freedom, and, most important, avoids shear locking, that has proven to be present in curved beams [?]. A possible shortcoming of Kirchhoff-Lovemodel is that high frequencies can be affected by some error. However, the use of technical beam theory in this context is questionable, since much more refined models are needed in that range.

A general space rod with torsion is considered. The Kirchhoff-Lovemodel presented is set in a Lagrangian description. The relevant equations and operators are evaluated in the intrinsic triad, either the reference or the updated (that are easily related one to the other). The finite

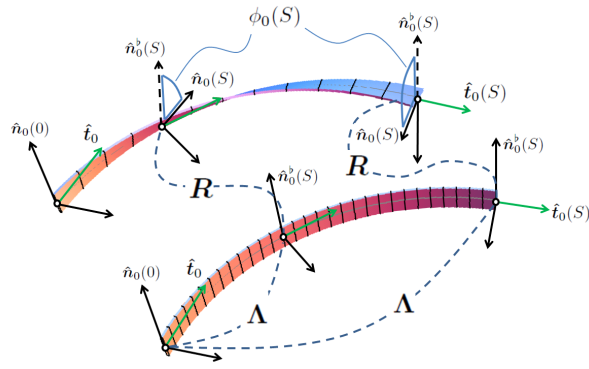


Figure 1: Intrinsic reference axes on the initial geometry of the rod

rotation of the intrinsic triad is described by an original map that decomposes the rotation in the rotation of the beam axis plus a torsional correction. When the velocity of rotation is evaluated, the bending and torsional velocities of rotation are automatically recovered.

Elastic behaviour is assumed for the beam, and the constitutive equations for the stress resultants are obtained consistently with the kinematic model. In the paper only linear elastic behavior is considered.

A detailed description of the Kirchhoff-Love space rod model can be found in [10]. Only a short summary, with emphasis on some more critical details, is given here.

2.1 Geometry and Kinematics

The rod is defined by the parametric domain \mathcal{A} , the parametric equation of the axis and by a unit vector field $\hat{\mathbf{n}}(S) : \mathcal{A} \rightarrow \mathbb{R}^3$ everywhere orthogonal to that curve. The parametric domain $\mathcal{A} =]0, L_0[$ coincides with the length of the axis in the reference configuration (assumed undeformed). The arc-length along the original rod axis is indicated by S . The position of the axis in a generic configuration is given by $\mathbf{p}(S)$. The original configuration is denoted by an index '0'.

The intrinsic triad is defined starting from the tangent vector to the curve, the unit vector field $\hat{\mathbf{t}} = \frac{d\mathbf{p}}{dS}$ (a hat indicates hereon a unit vector).

In the original configuration the unit triad is defined by the unit tangent $\hat{\mathbf{t}}_0 = \frac{d\mathbf{p}_0}{dS}$ plus the normal vector $\hat{\mathbf{n}}_0$ to the beam. This field is arbitrarily chosen (in general coincides with some inertia axis of the cross section) and is obtained starting from the definition of the normal in $S = 0$ by means of the combination of two rotations. The first, Λ , is the rotation around $\hat{\mathbf{t}}_0(0)$ that transforms $\hat{\mathbf{t}}_0(0)$ in $\hat{\mathbf{t}}_0(S)$ without drilling rotation, and is totally defined by the curve geometry. The second is a pure torsional rotation ϕ_0 around the unit tangent $\hat{\mathbf{t}}_0(S)$.

The unit local triad is completed by the unit vector

$$\hat{\mathbf{v}}_0(S) = \hat{\mathbf{t}}_0(S) \times \hat{\mathbf{n}}_0(S) \quad (1)$$

Then the initial geometry of the space rod is defined by the position vector $\mathbf{p}_0(S)$ and by the initial twist angle $\phi_0(S)$. (see figure 1).

The current centroid curve is given by

$$\mathbf{p}(S) = \mathbf{p}_0(S) + \mathbf{u}(S), \quad (2)$$

The unit spatial triad is defined starting from the current unit tangent vector field

$$\hat{\mathbf{t}}(S) = \frac{\mathbf{t}(S)}{\|\mathbf{t}(S)\|} = \frac{1}{\|\mathbf{t}(S)\|} \frac{d\mathbf{p}}{dS}. \quad (3)$$

The rotation of the cross section is given by two isometric operators, $\Lambda(\hat{\mathbf{t}}_0(S), \hat{\mathbf{t}}(S))$, a rotation without drilling that rotates the vector $\hat{\mathbf{t}}_0(S)$ on $\hat{\mathbf{t}}(S)$, and $\mathbf{R}(\hat{\mathbf{t}}(S), \phi(S))$ that gives the drilling rotation $\phi(S) : [0, L_0] \rightarrow \mathbb{R}$ around $\hat{\mathbf{t}}(S)$, that is also referred to as correction angle. The two operators are obtained particularizing *Euler-Rodriguez* formula

$$\mathbf{R} = \hat{\mathbf{e}} \otimes \hat{\mathbf{e}} + \cos[\varphi](\mathbf{I} - \hat{\mathbf{e}} \otimes \hat{\mathbf{e}}) + \sin[\varphi]\hat{\mathbf{e}} \times \mathbf{I}. \quad (4)$$

The unitary axial vector of the first rotation is $\hat{\mathbf{e}} = \frac{\hat{\mathbf{t}}_0 \times \hat{\mathbf{t}}}{\|\hat{\mathbf{t}}_0 \times \hat{\mathbf{t}}\|}$ while $\cos[\varphi] = \hat{\mathbf{t}}_0 \cdot \hat{\mathbf{t}}$ and $\sin[\varphi] = \|\hat{\mathbf{t}}_0 \times \hat{\mathbf{t}}\|$, therefore the formula (4) gives the representation

$$\Lambda(\hat{\mathbf{t}}_0, \hat{\mathbf{t}}) = (\hat{\mathbf{t}}_0 \cdot \hat{\mathbf{t}})\mathbf{I} + [\hat{\mathbf{t}}_0 \times \hat{\mathbf{t}}] \times \mathbf{I} + \frac{1}{1 + \hat{\mathbf{t}}_0 \cdot \hat{\mathbf{t}}} (\hat{\mathbf{t}}_0 \times \hat{\mathbf{t}}) \otimes (\hat{\mathbf{t}}_0 \times \hat{\mathbf{t}}) \quad (5)$$

The axial vector of the second rotation operator is $\hat{\mathbf{e}} = \hat{\mathbf{t}}$, and the correction angle is indicated by ϕ :

$$\mathbf{R}(\hat{\mathbf{t}}, \phi) = \mathbf{I} + \sin[\phi] \hat{\mathbf{t}} \times \mathbf{I} + (1 - \cos[\phi]) \hat{\mathbf{t}} \times [\hat{\mathbf{t}} \times \mathbf{I}]. \quad (6)$$

The remaining axes of the local triad are then

$$\hat{\mathbf{n}}(S) = \mathbf{R}(\hat{\mathbf{t}}, \phi) \Lambda(\hat{\mathbf{t}}_0, \hat{\mathbf{t}}) \hat{\mathbf{n}}_0(S), \quad \hat{\mathbf{v}}(S) = \mathbf{R}(\hat{\mathbf{t}}, \phi) \Lambda(\hat{\mathbf{t}}_0, \hat{\mathbf{t}}) \hat{\mathbf{v}}_0(S). \quad (7)$$

The construction described satisfies Kirchhoff-Love hypotheses $\hat{\mathbf{t}} \cdot \hat{\mathbf{n}} = \hat{\mathbf{t}} \cdot \hat{\mathbf{v}} = 0$. The current geometry of the rod is so defined by means of the two field $\{\mathbf{u}(S), \phi(S)\}$, so that it has four degrees of freedom.

It is possible to give a matrix representation of the operators \mathbf{R} , Λ , that are elements of the group SO^3 , in any of the reference frames. In the material frame the operator Λ assumes the form

$$\Lambda = \begin{pmatrix} \hat{\mathbf{t}} \cdot \hat{\mathbf{t}}_0 & -\hat{\mathbf{t}} \cdot \hat{\mathbf{n}}_0 & -\hat{\mathbf{t}} \cdot \hat{\mathbf{v}}_0 \\ \hat{\mathbf{t}} \cdot \hat{\mathbf{n}}_0 & \hat{\mathbf{t}} \cdot \hat{\mathbf{t}}_0 + \frac{(\hat{\mathbf{t}} \cdot \hat{\mathbf{v}}_0)^2}{1 + \hat{\mathbf{t}} \cdot \hat{\mathbf{t}}_0} & -\frac{(\hat{\mathbf{t}} \cdot \hat{\mathbf{n}}_0)(\hat{\mathbf{t}} \cdot \hat{\mathbf{v}}_0)}{1 + \hat{\mathbf{t}} \cdot \hat{\mathbf{t}}_0} \\ \hat{\mathbf{t}} \cdot \hat{\mathbf{v}}_0 & -\frac{(\hat{\mathbf{t}} \cdot \hat{\mathbf{n}}_0)(\hat{\mathbf{t}} \cdot \hat{\mathbf{v}}_0)}{1 + \hat{\mathbf{t}} \cdot \hat{\mathbf{t}}_0} & \hat{\mathbf{t}} \cdot \hat{\mathbf{t}}_0 + \frac{(\hat{\mathbf{t}} \cdot \hat{\mathbf{n}}_0)^2}{1 + \hat{\mathbf{t}} \cdot \hat{\mathbf{t}}_0} \end{pmatrix} \quad (8)$$

while the isometry \mathbf{R} is more effectively represented in the intermediate spatial frame $\{\hat{\mathbf{t}}, \hat{\mathbf{n}}^b = \Lambda \hat{\mathbf{n}}_0, \hat{\mathbf{v}}^b = \Lambda \hat{\mathbf{v}}_0\}$,

$$\mathbf{R} = \begin{pmatrix} 1 & 0 & 0 \\ 0 & \cos(\phi) & -\sin(\phi) \\ 0 & \sin(\phi) & \cos(\phi) \end{pmatrix} \quad (9)$$

Introducing the Lagrangian coordinates along the normal axes, the position of a generic point in the cross section is identified by the vector

$$\hat{\mathbf{p}}^*(S, \vartheta^n, \vartheta^\nu) = \mathbf{p}(S) + \boldsymbol{\xi} = \mathbf{p}(S) + \vartheta^n \hat{\mathbf{n}}(S) + \vartheta^\nu \hat{\mathbf{v}}(S). \quad (10)$$

The tangent vectors at the generic fibre of the rod are obtained differentiating equation (10)

$$\hat{\mathbf{t}}^* := \frac{\partial \hat{\mathbf{p}}^*}{\partial S} = \frac{\partial \mathbf{p}}{\partial S} + \vartheta^\nu \frac{\partial \hat{\boldsymbol{\nu}}}{\partial S} + \vartheta^n \frac{\partial \hat{\mathbf{n}}}{\partial S}, \quad \hat{\mathbf{n}}^* := \frac{\partial \hat{\mathbf{p}}^*}{\partial \vartheta^n} = \hat{\mathbf{n}}, \quad \hat{\boldsymbol{\nu}}^* := \frac{\partial \hat{\mathbf{p}}^*}{\partial \vartheta^\nu} = \hat{\boldsymbol{\nu}} \quad (11)$$

All the state variables are referred to the centroid line, using the push forward operators from the centroid line of the rod to the generic fibre, In the material and spatial configuration they are, respectively (the index \natural indicates the contravariant base vectors),

$$\begin{aligned} \mathbf{z} &= \mathbf{g}_\alpha^* \otimes \mathbf{g}^{\natural\alpha}, \quad \mathbf{g}_\alpha^* = \{\hat{\mathbf{t}}, \hat{\mathbf{n}}, \hat{\boldsymbol{\nu}}\}, \quad \mathbf{g}_\alpha = \{\mathbf{t}, \hat{\mathbf{n}}, \hat{\boldsymbol{\nu}}\} \\ \mathbf{z}_0 &= \mathbf{g}_{0\alpha}^* \otimes \mathbf{g}_0^{\natural\alpha}, \quad \mathbf{g}_{0\alpha}^* = \{\hat{\mathbf{t}}_0, \hat{\mathbf{n}}_0, \hat{\boldsymbol{\nu}}_0\}, \quad \mathbf{g}_{\alpha,0} = \{\mathbf{t}_0, \hat{\mathbf{n}}_0, \hat{\boldsymbol{\nu}}_0\} \end{aligned} \quad (12)$$

In the spatial configuration, the geometric curvatures of the beam are

$$\frac{1}{R_n} = \frac{1}{\|\mathbf{t}\|} \frac{d\hat{\mathbf{n}}}{dS} \cdot \hat{\mathbf{t}}, \quad \frac{1}{R_\nu} = \frac{1}{\|\mathbf{t}\|} \frac{d\hat{\boldsymbol{\nu}}}{dS} \cdot \hat{\mathbf{t}}, \quad \frac{1}{\tau} = \frac{1}{\|\mathbf{t}\|} \frac{d\hat{\mathbf{n}}}{dS} \cdot \hat{\boldsymbol{\nu}}, \quad (13)$$

the latter is the torsional curvature such that, in a non geodetic rod, it is

$$\hat{\mathbf{n}} \cdot \hat{\mathbf{t}}^* = -\frac{\vartheta^\nu}{\tau}, \quad \hat{\boldsymbol{\nu}} \cdot \hat{\mathbf{t}}^* = \frac{\vartheta^n}{\tau} \quad (14)$$

2.2 Tangent operator

The internal tangent operator and the velocity of deformation tensors are derived in detail in [10]. For the sake of completeness we summarize the main results.

The velocity of a generic point of the beam is

$$\dot{\hat{\mathbf{p}}}^* = \dot{\mathbf{u}} + \vartheta^n \dot{\hat{\mathbf{n}}} + \vartheta^\nu \dot{\hat{\boldsymbol{\nu}}}. \quad (15)$$

The motion of the intrinsic triad is obtained next. Since

$$\{\hat{\mathbf{t}}, \hat{\mathbf{n}}, \hat{\boldsymbol{\nu}}\} = \mathbf{Q}\{\hat{\mathbf{t}}_0, \hat{\mathbf{n}}_0, \hat{\boldsymbol{\nu}}_0\} \Rightarrow \{\dot{\hat{\mathbf{t}}}, \dot{\hat{\mathbf{n}}}, \dot{\hat{\boldsymbol{\nu}}}\} = \dot{\mathbf{Q}}\{\hat{\mathbf{t}}_0, \hat{\mathbf{n}}_0, \hat{\boldsymbol{\nu}}_0\} = \dot{\mathbf{Q}}\mathbf{Q}^{-1}\{\hat{\mathbf{t}}, \hat{\mathbf{n}}, \hat{\boldsymbol{\nu}}\}. \quad (16)$$

Evaluating we grt

$$\dot{\mathbf{Q}}\mathbf{Q}^T = \mathbf{R}\dot{\boldsymbol{\Lambda}}\boldsymbol{\Lambda}^T\mathbf{R}^T + \dot{\mathbf{R}}\mathbf{R}^T = \left(\dot{\hat{\mathbf{t}}} \otimes \hat{\mathbf{t}} - \hat{\mathbf{t}} \otimes \dot{\hat{\mathbf{t}}}\right) + \dot{\phi}\hat{\mathbf{t}} \times \mathbf{I}. \quad (17)$$

The spin vector $\boldsymbol{\omega}(S) : [0, L_0] \rightarrow \mathbb{R}^3$ associated to $\dot{\mathbf{Q}}$ is:

$$\boldsymbol{\omega} = \dot{\phi}\hat{\mathbf{t}} + \omega_n\hat{\mathbf{n}} + \omega_\nu\hat{\boldsymbol{\nu}} \quad (18)$$

with

$$\omega_n = \dot{\hat{\boldsymbol{\nu}}} \cdot \hat{\mathbf{t}} = -\frac{1}{\|\mathbf{t}\|} \frac{d\dot{\mathbf{u}}}{dS} \cdot \hat{\boldsymbol{\nu}}; \quad \omega_\nu = -\dot{\hat{\mathbf{n}}} \cdot \hat{\mathbf{t}} = \frac{1}{\|\mathbf{t}\|} \frac{d\dot{\mathbf{u}}}{dS} \cdot \hat{\mathbf{n}}. \quad (19)$$

With the aid of the rotation vector $\boldsymbol{\omega}$, the velocity of the intrinsic triad takes the form

$$\begin{aligned} \dot{\hat{\mathbf{t}}} &= \omega_\nu\hat{\mathbf{n}} - \omega_n\hat{\boldsymbol{\nu}} \\ \dot{\hat{\mathbf{n}}} &= -\omega_\nu\hat{\mathbf{t}} + \dot{\phi}\hat{\boldsymbol{\nu}} \\ \dot{\hat{\boldsymbol{\nu}}} &= \omega_n\hat{\mathbf{t}} - \dot{\phi}\hat{\mathbf{n}}. \end{aligned} \quad (20)$$

We observe, for later use, that the continuity of the beam is guaranteed if the velocities of the torsional rotation $\dot{\phi}$ and of the bending rotations ω_n, ω_ν are continuous. In particular, the continuity of the bending rotations requires the continuity of the norm $\|\mathbf{t}\|$ of the tangent vector, and the continuity of the normal components of the line gradient of the velocity.

The derivative along the arc length of $\boldsymbol{\omega}$ is the curvature vector

$$\frac{1}{\|\mathbf{t}\|} \frac{d\boldsymbol{\omega}}{dS} = \dot{\chi}_t \hat{\mathbf{t}} + \dot{\chi}_n \hat{\mathbf{n}} + \dot{\chi}_\nu \hat{\boldsymbol{\nu}} \quad (21)$$

$$\begin{aligned} \dot{\chi}_t &= \frac{1}{\|\mathbf{t}\|} \frac{d\dot{\phi}}{dS} + \frac{\omega_n}{R_n} + \frac{\omega_\nu}{R_\nu} = \frac{1}{\|\mathbf{t}\|} \frac{d\hat{\mathbf{n}}}{dS} \cdot \hat{\boldsymbol{\nu}} \\ \dot{\chi}_n &= \frac{1}{\|\mathbf{t}\|} \frac{d\omega_n}{dS} - \frac{\omega_\nu}{\tau} - \frac{\dot{\phi}}{R_n} = \frac{1}{\|\mathbf{t}\|} \frac{d\hat{\mathbf{t}}}{dS} \cdot \hat{\mathbf{n}} \\ \dot{\chi}_\nu &= \frac{1}{\|\mathbf{t}\|} \frac{d\omega_\nu}{dS} + \frac{\omega_n}{\tau} - \frac{\dot{\phi}}{R_\nu} = \frac{1}{\|\mathbf{t}\|} \frac{d\hat{\mathbf{t}}}{dS} \cdot \hat{\mathbf{n}}\hat{\boldsymbol{\nu}}. \end{aligned} \quad (22)$$

The bending velocity of curvature can be related to the second covariant derivative of the velocity of displacement vector, $\frac{1}{\|\mathbf{t}\|^2} \frac{d^2 \dot{\mathbf{u}}}{dS^2} = \frac{1}{\|\mathbf{t}\|} \frac{d}{dS} \left(\frac{1}{\|\mathbf{t}\|} \frac{d\dot{\mathbf{u}}}{dS} \right)$, in the form

$$\begin{aligned} \dot{\chi}_n &= -\frac{1}{\|\mathbf{t}\|^2} \frac{d^2 \dot{\mathbf{u}}}{dS^2} \cdot \hat{\boldsymbol{\nu}} - \frac{\dot{\phi}}{R_n} - \frac{1}{\|\mathbf{t}\|^2} \dot{\mathbf{t}} \cdot \mathbf{t} \frac{1}{R_\nu} \\ \dot{\chi}_\nu &= \frac{1}{\|\mathbf{t}\|^2} \frac{d^2 \dot{\mathbf{u}}}{dS^2} \cdot \hat{\mathbf{n}} - \frac{\dot{\phi}}{R_\nu} + \frac{1}{\|\mathbf{t}\|^2} \dot{\mathbf{t}} \cdot \mathbf{t} \frac{1}{R_n}. \end{aligned} \quad (23)$$

2.3 The velocity of deformation operator for a Kirchhoff-Love rod

The application in this paper are limited to infinitesimal deformations, so we only need to derive the velocity of deformation tensor. Denoting with \mathbf{F} the gradient of deformation from the reference configuration of the axis to its current configuration i.e. $\mathbf{F} = \mathbf{g}_\alpha \otimes \mathbf{g}_0^{\alpha} = \mathbf{t} \otimes \mathbf{t}_0 + \hat{\mathbf{n}} \otimes \hat{\mathbf{n}}_0 + \hat{\boldsymbol{\nu}} \otimes \hat{\boldsymbol{\nu}}_0$ the pull-back of the velocity of deformation on the reference configuration $\dot{\mathbf{E}} = \dot{E}_{\alpha\beta} \mathbf{g}_0^{\alpha} \otimes \mathbf{g}_0^{\beta} = \text{sym} \left((\mathbf{z}\mathbf{F})^T \dot{\mathbf{z}}\mathbf{F} \right)$ has the components

$$\dot{\mathbf{E}} = \frac{1}{2} \begin{pmatrix} 2 \dot{\mathbf{t}} \cdot \dot{\mathbf{t}} & -\vartheta^\nu \left(\frac{d\hat{\mathbf{n}}}{dS} \cdot \hat{\boldsymbol{\nu}} + \frac{d\hat{\mathbf{n}}}{dS} \cdot \dot{\hat{\boldsymbol{\nu}}} \right) & \vartheta^n \left(\frac{d\hat{\mathbf{n}}}{dS} \cdot \hat{\boldsymbol{\nu}} + \frac{d\hat{\mathbf{n}}}{dS} \cdot \dot{\hat{\boldsymbol{\nu}}} \right) \\ -\vartheta^\nu \left(\frac{d\hat{\mathbf{n}}}{dS} \cdot \hat{\boldsymbol{\nu}} + \frac{d\hat{\mathbf{n}}}{dS} \cdot \dot{\hat{\boldsymbol{\nu}}} \right) & 0 & 0 \\ \vartheta^n \left(\frac{d\hat{\mathbf{n}}}{dS} \cdot \hat{\boldsymbol{\nu}} + \frac{d\hat{\mathbf{n}}}{dS} \cdot \dot{\hat{\boldsymbol{\nu}}} \right) & 0 & 0 \end{pmatrix} \quad (24)$$

The components of the velocity of deformation are readily found performing the derivatives in (24). Using the results of equation (22), the components of the shear deformation velocity, the off-diagonal terms of tensor (24), are

$$\dot{\gamma}_{\hat{\mathbf{n}}\mathbf{t}}^* = -\vartheta^\nu \dot{\chi}_t \quad \dot{\gamma}_{\hat{\boldsymbol{\nu}}\mathbf{t}}^* = \vartheta^n \dot{\chi}_t \quad (25)$$

The result definitions (19) and the identity

$$\hat{\mathbf{t}} \times \frac{d\hat{\mathbf{t}}}{dS} = \|\mathbf{t}\| \left(-\frac{\hat{\mathbf{n}}}{R_\nu} + \frac{\hat{\boldsymbol{\nu}}}{R_n} \right) \quad (26)$$

allow to get a representation of $\dot{\chi}_t$ in terms of the Lagrangian generalized velocity vector $\dot{\mathbf{q}} = \{\dot{\mathbf{u}}, \dot{\phi}\}$:

$$\dot{\chi}_t = \frac{1}{\|\mathbf{t}\|} \left(\hat{\mathbf{t}} \times \frac{d\hat{\mathbf{t}}}{dS} \right) \cdot \frac{d\dot{\mathbf{u}}}{dS} + \frac{d\dot{\phi}}{dS}. \quad (27)$$

Using expression (11) and disregarding the terms quadratic in the normal coordinates, the Lagrangian axial deformation of the generic fibre can be written as

$$\overset{*}{\mathbf{t}} \cdot \overset{*}{\mathbf{t}} \approx \mathbf{t} \cdot \mathbf{t} + 2\|\mathbf{t}\|^2 \frac{\vartheta^n}{R_n} + 2\|\mathbf{t}\|^2 \frac{\vartheta^\nu}{R_\nu} \quad (28)$$

The axial velocity is then given by

$$\begin{aligned} \overset{\cdot}{\mathbf{t}} \cdot \overset{\cdot}{\mathbf{t}} &= \dot{\mathbf{t}} \cdot \dot{\mathbf{t}} + \vartheta^n \left(-\frac{d\omega_\nu}{dS} \|\mathbf{t}\| + \frac{\dot{\phi}}{R_\nu} \|\mathbf{t}\|^2 - \frac{\omega_n}{\tau} \|\mathbf{t}\| + \frac{\dot{\mathbf{t}} \cdot \dot{\mathbf{t}}}{R_n} \right) \\ &+ \vartheta^\nu \left(\frac{d\omega_n}{dS} \|\mathbf{t}\| - \frac{\dot{\phi}}{R_n} \|\mathbf{t}\|^2 - \frac{\omega_\nu}{\tau} \|\mathbf{t}\| + \frac{\dot{\mathbf{t}} \cdot \dot{\mathbf{t}}}{R_\nu} \right) \end{aligned} \quad (29)$$

that can be cast in the form:

$$\overset{\cdot}{\mathbf{t}} \cdot \overset{\cdot}{\mathbf{t}} = \dot{\epsilon}_r + \dot{\boldsymbol{\chi}}^\perp \cdot \boldsymbol{\xi} \|\mathbf{t}\| \quad (30)$$

with the notations

$$\begin{aligned} \dot{\epsilon}_r &= \dot{\mathbf{t}} \cdot \dot{\mathbf{t}} \left(1 + \frac{\theta^n}{R_n} + \frac{\theta^\nu}{R_\nu} \right) = \dot{\mathbf{t}} \cdot \dot{\mathbf{t}} \left(1 - \boldsymbol{\xi} \cdot \frac{d\hat{\mathbf{t}}}{dS} \frac{1}{\|\mathbf{t}\|} \right) \\ \dot{\boldsymbol{\chi}}^\perp &= \hat{\mathbf{t}} \times \dot{\boldsymbol{\chi}} \\ \boldsymbol{\xi} &= \theta_n \hat{\mathbf{n}} + \theta_\nu \hat{\boldsymbol{\nu}} \end{aligned} \quad (31)$$

An alternative expression for the axial velocity of deformation, using equation (23) is

$$\begin{aligned} \overset{\cdot}{\mathbf{t}} \cdot \overset{\cdot}{\mathbf{t}} &= \dot{\epsilon} + \boldsymbol{\xi} \cdot \dot{\boldsymbol{\chi}}_r^\perp \|\mathbf{t}\| \\ \dot{\epsilon} &= \dot{\mathbf{t}} \cdot \dot{\mathbf{t}} \quad \|\mathbf{t}\| \dot{\boldsymbol{\chi}}_r^\perp = -\frac{d^2 \dot{\mathbf{u}}}{dS^2} + \left(\hat{\mathbf{t}} \times \frac{d\dot{\mathbf{t}}}{dS} \right) \|\mathbf{t}\| \dot{\phi}. \end{aligned} \quad (32)$$

3 EQUILIBRIUM OPERATOR FOR KIRCHHOFF-LOVE ROD

3.1 Virtual Power Identity

The equilibrium operator is obtained from the principle of virtual power. The representation of the internal power on the reference configuration is:

$$P_{int} = \int_{L_0} \left(\int_{\mathcal{A}} \mathbf{S} : \dot{\mathbf{E}} d\mathcal{A} \right) dS, \quad (33)$$

with $\mathbf{S} = S^{\alpha\beta} \mathbf{g}_{0\alpha} \otimes \mathbf{g}_{0\beta}$ the second Piola-Kirchhoff stress tensor, given by

$$\mathbf{S} = \det(\mathbf{zF})(\mathbf{zF})^{-1} \boldsymbol{\Sigma}^* (\mathbf{zF})^{-T} \quad (34)$$

Its components on the reference unitary centroid triads are

$$S = \begin{pmatrix} S^{tt} & S^{tn} & S^{t\nu} \\ S^{nt} & 0 & 0 \\ S^{\nu t} & 0 & 0 \end{pmatrix}. \quad (35)$$

Substituting the components of the velocity of deformation in (??), one has

$$\begin{aligned} P_{int} &= \int_{L_0} \left(\int_{\mathcal{A}} S^{tt} (\dot{\varepsilon} - \vartheta^n \dot{\chi}_\nu \|\mathbf{t}\| + \vartheta^\nu \dot{\chi}_n \|\mathbf{t}\| + (S^{\nu t} \vartheta^n - S^{nt} \vartheta^\nu) \dot{\chi}_t) d\mathcal{A} \right) dS \\ &= \int_{L_0} (N \dot{\varepsilon} + \mathbf{M} \cdot \dot{\boldsymbol{\chi}}_r \|\mathbf{t}\| + M_t \dot{\chi}_t) dS \\ &= \int_{L_0} \left(N \left(\frac{d\dot{\mathbf{u}}}{dS} \cdot \mathbf{t} \right) + M_n \left(-\frac{d^2 \dot{\mathbf{u}}}{dS^2} \cdot \hat{\boldsymbol{\nu}} - \frac{\|\mathbf{t}\|^2}{R_n} \dot{\phi} \right) \right) + \\ &\quad M_\nu \left(\frac{d^2 \dot{\mathbf{u}}}{dS^2} \cdot \hat{\mathbf{n}} - \frac{\|\mathbf{t}\|^2}{R_\nu} \dot{\phi} \right) + M_t \left(\frac{d\dot{\phi}}{dS} + \frac{1}{\|\mathbf{t}\|} \frac{d\dot{\mathbf{u}}}{dS} \left(\hat{\mathbf{t}} \times \frac{d\hat{\mathbf{t}}}{dS} \right) \right) dS, \end{aligned} \quad (36)$$

where the following definitions have been introduced:

$$\begin{aligned} N &= \int_{\mathcal{A}} S^{tt} d\mathcal{A}, \\ \mathbf{M} &= \int_{\mathcal{A}} \boldsymbol{\xi} \times (S^{tt} \hat{\mathbf{t}}) d\mathcal{A}, \\ M_t &= \int_{\mathcal{A}} (S^{\nu t} \vartheta^n - S^{nt} \vartheta^\nu) d\mathcal{A}. \end{aligned} \quad (37)$$

3.2 Constitutive operator of the rod

We assume that the rod remains elastic, and, since only small deformation problems are treated in this work, we consider only linear elastic behaviour. Therefore the increment of the second Piola-Kirchhoff stress tensor are given by

$$\begin{aligned} \dot{S}^{tt} &= E (\dot{\mathbf{t}} \cdot \dot{\mathbf{t}}) = \mathcal{E} \left[\dot{\varepsilon} \left(1 + \frac{\vartheta^n}{R_n} + \frac{\vartheta^\nu}{R_\nu} \right) - \vartheta^n \dot{\chi}_\nu \|\mathbf{t}\| + \vartheta^\nu \dot{\chi}_n \|\mathbf{t}\| \right] \\ &= E \left[\dot{\mathbf{t}} \cdot \mathbf{t} + \vartheta^n \left(-\frac{d^2 \dot{\mathbf{u}}}{dS^2} \cdot \hat{\mathbf{n}} + \|\mathbf{t}\|^2 \frac{\dot{\phi}}{R_\nu} \right) + \vartheta^\nu \left(-\frac{d^2 \dot{\mathbf{u}}}{dS^2} \cdot \hat{\boldsymbol{\nu}} - \|\mathbf{t}\|^2 \frac{\dot{\phi}}{R_n} \right) \right] \\ \dot{S}^{tn} &= -G \vartheta^\nu \dot{\chi}_t \quad \dot{S}^{t\nu} = G \vartheta^n \dot{\chi}_t. \end{aligned} \quad (38)$$

4 NUMERICAL FORMULATION

4.1 B-Spline interpolation

The weak equilibrium equations (36) are discretized approximating the geometric fields that define the problem with B-splines. In the following, even though splines are not interpolatory, we shall refer to B-spline interpolation for convenience. A single B-Spline curve of degree p is defined as

$$\mathbf{C}(\lambda) = \sum_{i=1}^n N_{i,p}(\lambda) \mathbf{P}_i \quad (39)$$

where $\mathbf{P}_i = \{P_{ix}, P_{iy}, P_{iz}\}$ are the cartesian components of n control points, and $N_{i,p}$ are the n B-Spline basis functions of degree p defined on a non periodic knot vector. An open knot vector is a non decreasing sequence of m real numbers, the parametric coordinate $\lambda_j, j = 1, \dots, m$, with $m = n + p + 1$,

$$\Xi = \left\{ \underbrace{a, \dots, a}_{p+1}, \underbrace{\lambda_{p+2}, \dots, \lambda_{m-(p+2)}}_{m-2(p+1)}, \underbrace{b, \dots, b}_{p+1} \right\}$$

The global interval $[a, b]$ is called the patch. A B-spline curve has C^{p-1} parametric continuity in each patch.

In the case the knot vector has no internal knots the basis functions reduce to the Bernstein polynomials, so that the B-Spline interpolation is a generalization of the Bezier's interpolation.

An isoparametric interpolation is used, that is, both the initial geometry ($\mathbf{p}(S)$ and $\phi_0(S)$) and the degrees of freedom of the model, i.e., the displacement \mathbf{u} and the torsional rotation ϕ , are interpolated by means of the same B-splines:

$$\begin{aligned} \mathbf{q}(\lambda) &= \{p_x(\lambda), p_y(\lambda), p_z(\lambda), \phi(\lambda)\} \\ p_\alpha(\lambda) &= \sum_{i=1}^n N_{i,p} P_{\alpha i} = \hat{\mathbf{M}} \mathbf{P}_\alpha \quad \phi(\lambda) = \sum_{i=1}^n N_{i,p} \Phi_i = \hat{\mathbf{M}} \Phi \end{aligned} \quad (40)$$

so that $\mathbf{p}(\lambda) = \mathbf{M} \mathbf{P}$ with

$$\mathbf{M} = \begin{bmatrix} \hat{\mathbf{M}} & 0 & 0 \\ 0 & \hat{\mathbf{M}} & 0 \\ 0 & 0 & \hat{\mathbf{M}} \end{bmatrix} \quad (41)$$

where the matrix $\hat{\mathbf{M}} = [N_{1,p}, \dots, N_{n,p}]$. The first and the second derivatives of the basis functions are

$$\mathbb{B} = \frac{d\mathbf{M}}{d\lambda} \quad \mathbb{D} = \frac{d^2\mathbf{M}}{d\lambda^2}. \quad (42)$$

while the interpolation of the second gradient along the arc-length, according to expression (23)

is

$$\begin{aligned} \frac{d^2 \bullet}{dS^2} &= \frac{1}{\|\mathbf{t}_0\|} \frac{d}{d\lambda} \left(\frac{1}{\|\mathbf{t}_0\|} \frac{d\bullet}{d\lambda} \right) - \frac{1}{\|\mathbf{t}_0\|^2} \frac{1}{\|\mathbf{t}\|^2} \left(\frac{d\mathbf{t}}{d\lambda} \cdot \mathbf{t} \right) \frac{d\bullet}{d\lambda} = \\ & \frac{1}{\|\mathbf{t}_0\|^2} \mathbb{D} - \frac{\mathbb{D}\mathbf{P} \cdot \mathbb{B}\mathbf{P}}{\|\mathbf{t}\|^2 \|\mathbf{t}_0\|^2} \mathbb{B} = \mathbb{X} \end{aligned} \quad (43)$$

The cartesian components of the sectional axes $\hat{\mathbf{n}}, \hat{\boldsymbol{\nu}}$ are given by expressions (??), and are interpolated accordingly, and will be indicated as

$$\mathbf{n} = \mathbb{N}(\mathbf{P}) \quad \boldsymbol{\nu} = \mathbb{V}(\mathbf{P}). \quad (44)$$

It is interesting to note that the initial geometry is interpolated in this work with the same precision as the degrees of freedom, so no special effort is devoted to reduce the interpolation error on the initial tangent vectors.

5 PARAMETRIZATION OF THE ROTATIONS FOR PATCH CONTINUITY

It is common in engineering analysis that assemblies of several rods have to be considered, joined at the ends in such a way that they keep a geometric continuity on the angle formed by the tangents. It is also useful to recur to multipatch descriptions when the properties of the rod sudden change, like for soldered beams of different cross-section, or when the geometry is too complex for being satisfactorily approximated by a single patch. The problem of joining patches with geometric continuity has recently received some attention [?, ?], and weak formulations of the geometric constraints or special bridging elements have been proposed. Here we propose an intrinsic formulation for the G^1 continuity. The main idea moves from the observation that the geometric curve at the first and the last control point is interpolated and is tangent to the first and last segments of the control polygon, see figure ??.

We assume that the initial positioning of the patches satisfy parametric C^1 continuity at the joints, that guarantees that the tangent vector \mathbf{t} is everywhere continuous, in direction and norm.

A polar re-parametrization of the second and second last points of the control polygon is proposed, in the sense that the angles at the ends and the distance between the first and the second and the last second and the last control points are assumed as Lagrangian parameters of these points. In this manner a C^0 assembly on the angle at the ends ensures the G^1 -continuity for the centroid curve, and it is possible an easy global assemblage of the stiffness matrix.

The details will be reported in a paper in preparation, but, limiting ourselves to the case of linearized kinematics, the parametrization amounts to a basis transformation for the dof's of the first and last two control points. Focusing on the first two control points, let $(\dot{\mathbf{q}}_1, \dot{\mathbf{q}}_2) = (\dot{P}_{1x}, \dot{P}_{1y}, \dot{P}_{1z}, \dot{\phi}_1, \dot{P}_{2x}, \dot{P}_{2y}, \dot{P}_{2z}, \dot{\phi}_2)$ be the dof's of the first two nodes in the standard B-spline interpolation, and let

$(\dot{\mathbf{q}}_1, \dot{\tilde{\mathbf{q}}}) = (\dot{P}_{1x}, \dot{P}_{1y}, \dot{P}_{1z}, \dot{\omega}_{1x}, \dot{\omega}_{1y}, \dot{\omega}_{1z}, \dot{\rho}_2, \dot{\phi}_2)$ be the re-parametrized dof's of the first two nodes, where the rotation of the extremity of the rod are projected on a material external reference frame.

The basis transformation is obtained by the relation

$$\dot{\mathbf{P}}_2 = \dot{\mathbf{P}}_1 + \boldsymbol{\omega} \times (\mathbf{P}_2 - \mathbf{P}_1) + \dot{\rho} \|\mathbf{P}_2 - \mathbf{P}_1\|. \quad (45)$$

6 EXAMPLES

The performance of the model is tested with some applications presented in this section. Particularly, the convergence rate of the procedure and consideration on locking will be given with respect to the numerical results that have been found. The applications have been carefully chosen in order to highlight these phenomena.

6.1 Multipatch pretwisted beam

The first example concerns a benchmark proposed by McNeal [14] on a pretwisted cantilever, with linear variation of the twist angle, with two loading conditions, see figures 2(a), 2(b). The data are $L = 12$, $E = 29 * 10^6$, $h_n = 1.1$, $h_\nu = 0.32$ $\phi(S) = \frac{\pi}{2} \frac{\lambda}{L}$, with $\lambda \in [0, 1]$. In figures 2(c), 2(d) are shown the convergence rate of the error of the tip displacements dual to the applied load with respect to the exact value for increasing number of patches in the case of G^1 -multipatch analysis and increasing the control point by h -refinement in the case of a single B-Spline analysis (in these figures as well as in the following, on the abscissa is reported the number of degrees of freedom, function of the number of patches). The convergence rate is function of the degree of the polynomial interpolation, but for single patch B-Spline models the convergence is faster than for the multipatch case.

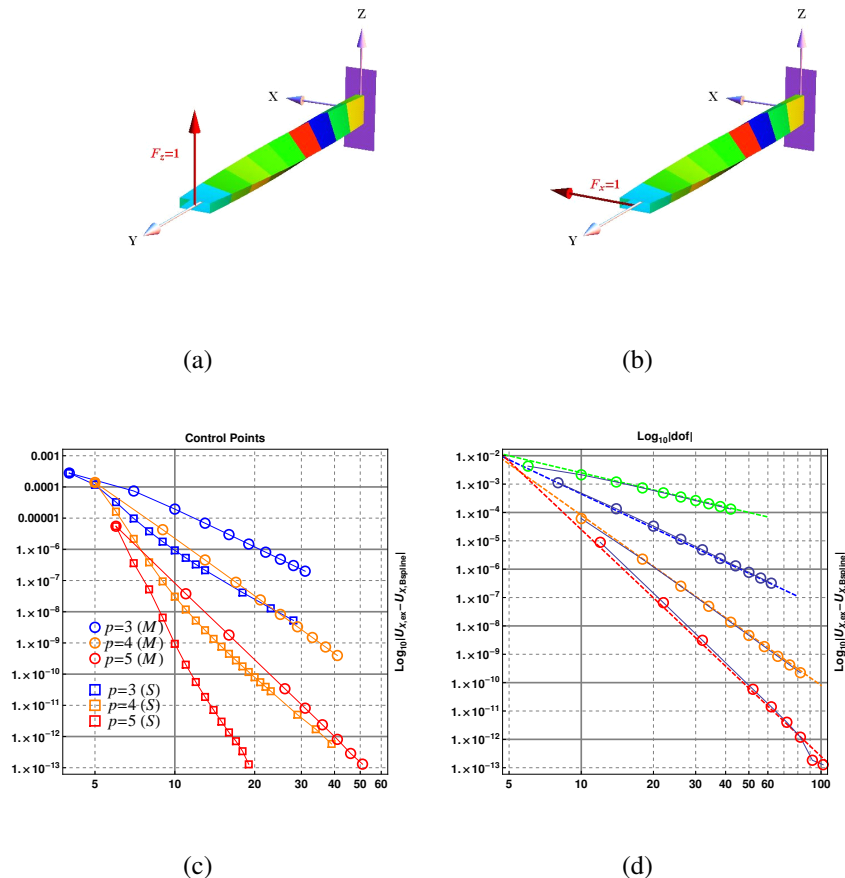


Figure 2: 3D cantilever pre-twisted beam; 2(a) initial geometry load case-1; 2(b) initial geometry load case-2; 2(c) convergence's error for the $u_z(L)$ at the free end; 2(d) convergence's error for the $u_x(L)$ at the free end (p=2 green, p=3 blue, p=4 orange, and p=5 red, p is the polynomial degree).

6.2 Multi- and single-patch 3D-cantilever arch with a point force

The next example concerns a geodetic horizontal arch loaded at the tip by a vertical force $F = \{0, 0, -1\}, [kN]$. The radius of the centroid curve is $R = 1 [m]$ the section is rectangular with $h_n = 0.1$ and $h_v = 0.01 [m]$ respectively, and $E = 1.999 \times 10^8 [kN/m^2]$, figure 3(a). Figures 3(b) and subsequent show the convergence error on the tip displacement and rotation, and for the bending moment, twisting moment and shear force at the constrained end. It is interesting to note that while for few patches the convergence rate is equal to the splines degree p , as in the case of single patch analysis, for larger number of patches the convergence rate becomes smaller, tending to $p - 1$.

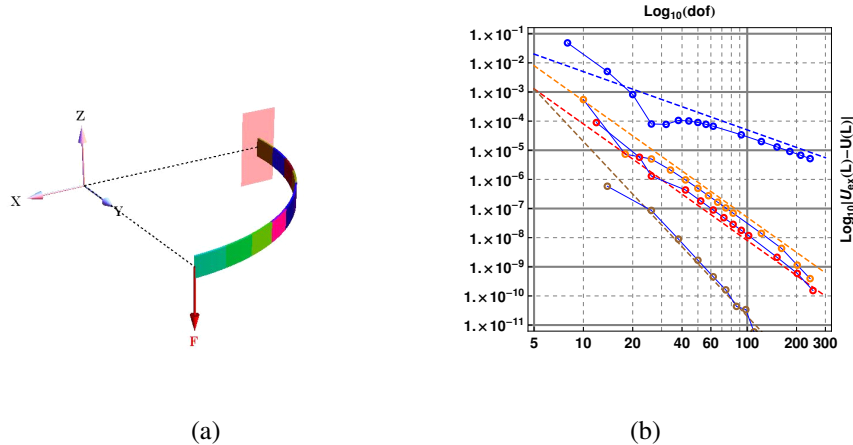


Figure 3: 3D cantilever arch with a point force at the end; 3(a) initial geometry, 3(b) convergence's error for the vertical displacement at the free end $u_z(L)$, for $R/h_n = 100$ ($p=2$ green, $p=3$ blue, $p=4$ orange, $p=5$ red, and $p=6$ brown, p is the polynomial degree).

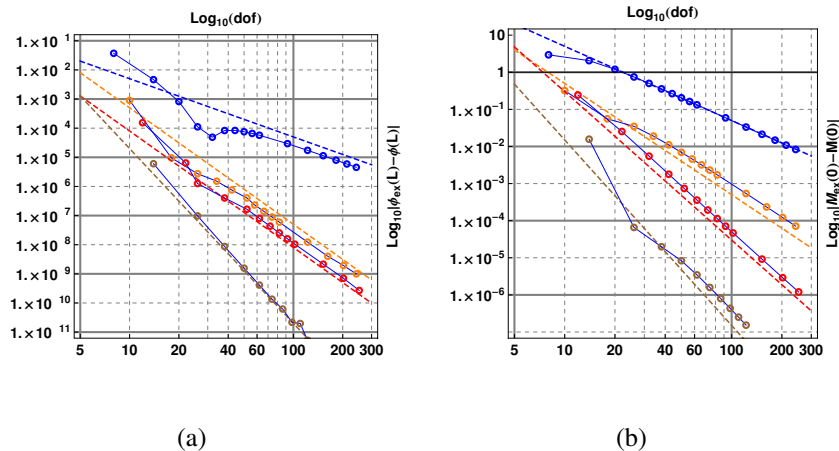


Figure 4: Figure-4(a) error's convergence for the free end rotation $\phi(L)$, Figure-4(b) error's convergence for the bending moment at the constrained end, for $R/h_n = 100$ ($p=2$ green, $p=3$ blue, $p=4$ orange, $p=5$ red, and $p=6$ brown, p is the polynomial degree).

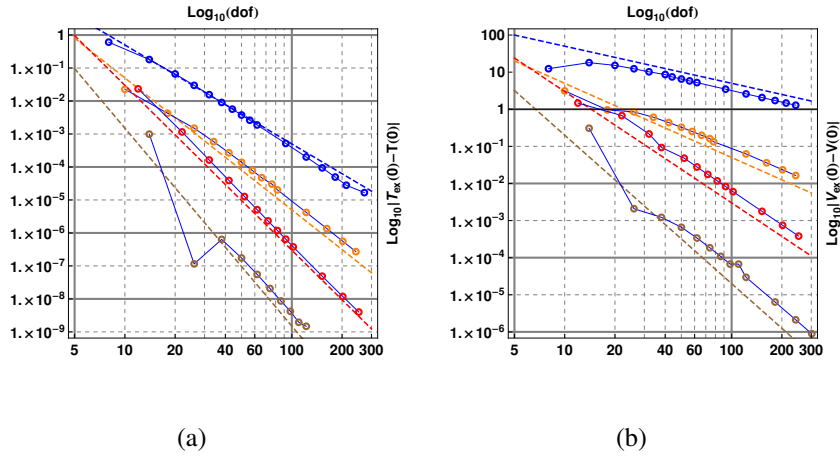


Figure 5: Figure-5(a) error's convergence for the twisting moment at the constrained end, Figure-5(b) error's convergence for the shear force at the constrained end, for $R/h_n = 100$ (p=2 green, p=3 blue, p=4 orange, p=5 red, and p=6 brown, p is the polynomial degree).

6.3 2D-cantilever arch with a couple

The data considered are $R = 1 [m]$, $h_n = 0.1 [m]$, $h_v = 0.01 [m]$, $E = 1.999 \times 10^8 [KN/m^2]$. In this example, in addition to the analysis of convergence, locking is analysed. Note that in this case membrane locking is expected for standard FE models. A couple $M_h = (\frac{h}{R})^3$ is applied at the tip. in this manner the vertical displacement for different value of M_h is h -independent. A multi-patch interpolation is used. The convergence analysis reported in figure 6(b) substantially confirms the conclusion drawn at the end of the previous section.

In figure-6.3 we consider the influence of the slenderness ratio R/h on the solution for a couple. The horizontal line represent the exact solution for any value of M_h . It can be observed that for slenderness ratios higher than a threshold, the solution curve for the tip displacement deviates from the exact solution. The threshold for the slenderness is larger the higher the spline degree. The example shows the existence of locking phenomena in the isogeometric interpolation.

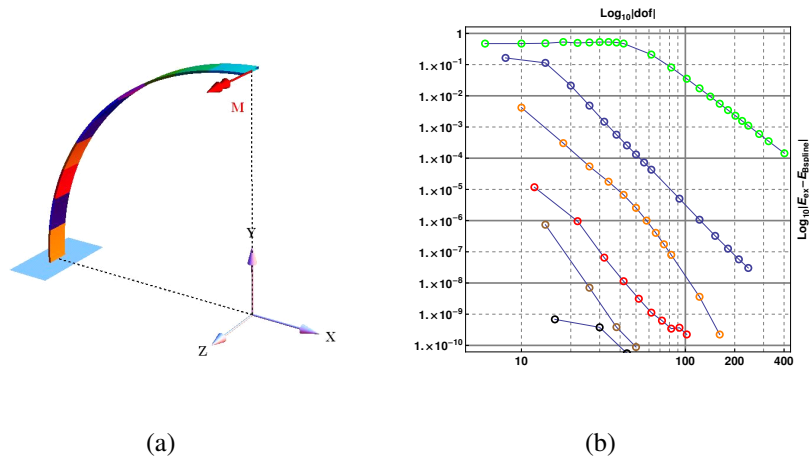


Figure 6: 3D cantilever arch with a couple at the end; 6(a) initial geometry, 6(b) convergence's error in energy, for $R/h_n = 100$ (p=2 green, p=3 blue, p=4 orange, p=5 red, p=6 brown and p=7 black, p is the polynomial degree).

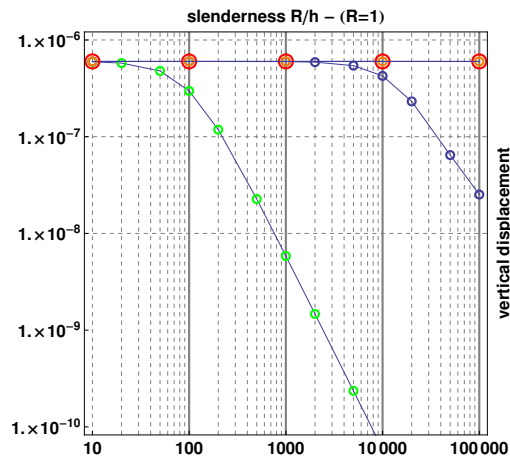


Figure 7: Influence of the slenderness ratio on the vertical displacement of the free end, ($p=2$ green, $p=3$ blue, $p=4$ orange, $p=5$ red, p is the polynomial degree).

6.4 2D-cantilever arch with a point force

In this section it's considered the case of a cantilever arch with a transverse force applied at the tip. The geometry is defined by $R = 1 [m]$, $h_n = 0.1 [m]$, $h_v = 0.01 [m]$, $E = 1.999 * 10^8 [KN/m^2]$. In figure 8(b), with reference to the vertical displacement of the loaded point, it is presented a comparison for the convergence rate between a G^1 -multipatch analysis and a h-refinement in a B-Spline single patch. The higher continuity of the latter case generates improves the convergence's rate. In figure-9 we consider the influence of the slenderness ratio $\frac{R}{h}$ on the vertical displacement of the free end, for a fixed number of degree of freedom and for a fixed force $F = 1 [KN]$, considering both kinds of interpolation. Also in this case locking arises when the+ slenderness ratio exceeds a threshold value.

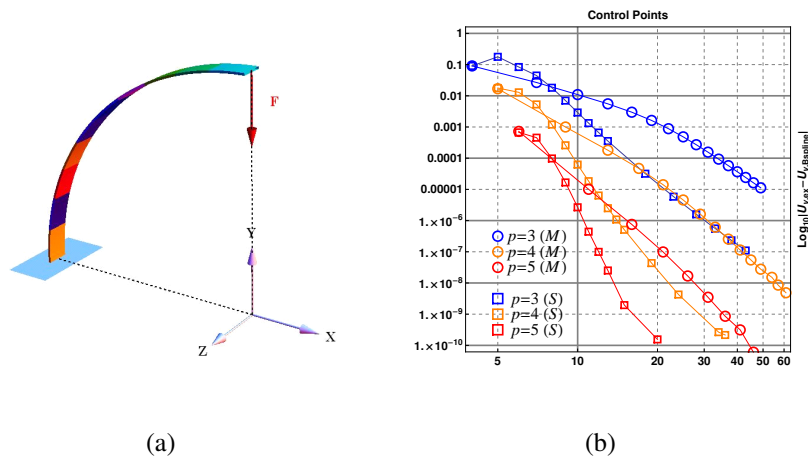


Figure 8: 2D cantilever arch with a point force at the end; 8(a) initial geometry, 8(b) convergence's error in energy, for $R/h_n = 100$ ($p=3$ blue, $p=4$ orange and $p=5$ red p is the polynomial degree); the \circ -markers for the G^1 -multipatch and the \square -marker for the h-refinement analysis.

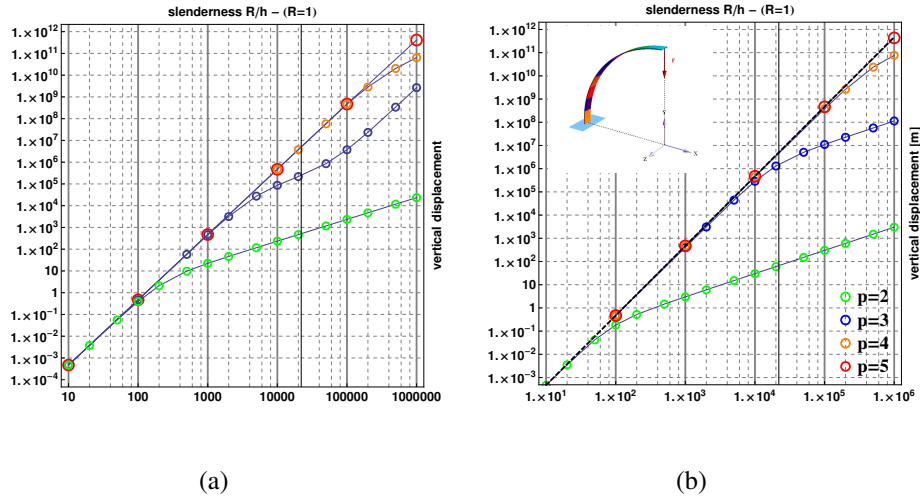


Figure 9: Influence of the slenderness ratio on the vertical displacement of the free end; 9(a) G^1 -multipatch analysis; 9(b) h -refinement in single B-Spline patch; ($p=2$ green, $p=3$ blue, $p=4$ orange, $p=5$ red, p is the polynomial degree).

6.5 A B-Splines multipatch 3D-helix

In this sub section it is considered the case of a helix of equation

$$x(\alpha) = R(\alpha) \cos(\pi - \alpha), \quad y(\alpha) = R(\alpha) \sin(\pi - \alpha), \quad \alpha \in [0, 1] \quad (46)$$

and the radius $R(\alpha) = \frac{R(1)-R(0)}{6\pi} \alpha + R(0)$, with $R(1) = 0.25R(0)$ and $R(0) = 1$. The section is rectangular with dimensions $h_n = 0.1 [m]$, $h_v = 0.01 [m]$, $E = 1.999 * 10^8 [KN/m^2]$. The vector $\hat{n} = \{1, 0, 0\}$ and $\hat{v} = \hat{t} \times \hat{n}$. The helix is loaded by a vertical point force at the free end $\mathbf{F} = \{0, 0, -1\}$. The deformed centroid curve is shown in figure 10(a) and the correction angle ϕ is shown in figure 10(b).

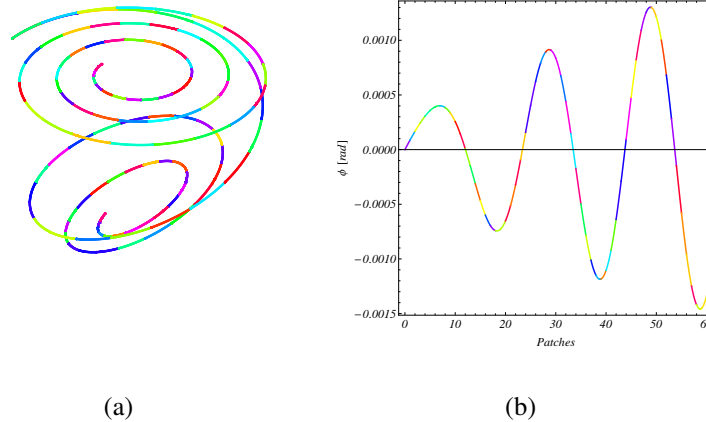


Figure 10: 10(a) Initial geometry and magnified deformed configuration; 10(b) correction angle ϕ .

The bending moment and the twisting moment are shown in the figure 11

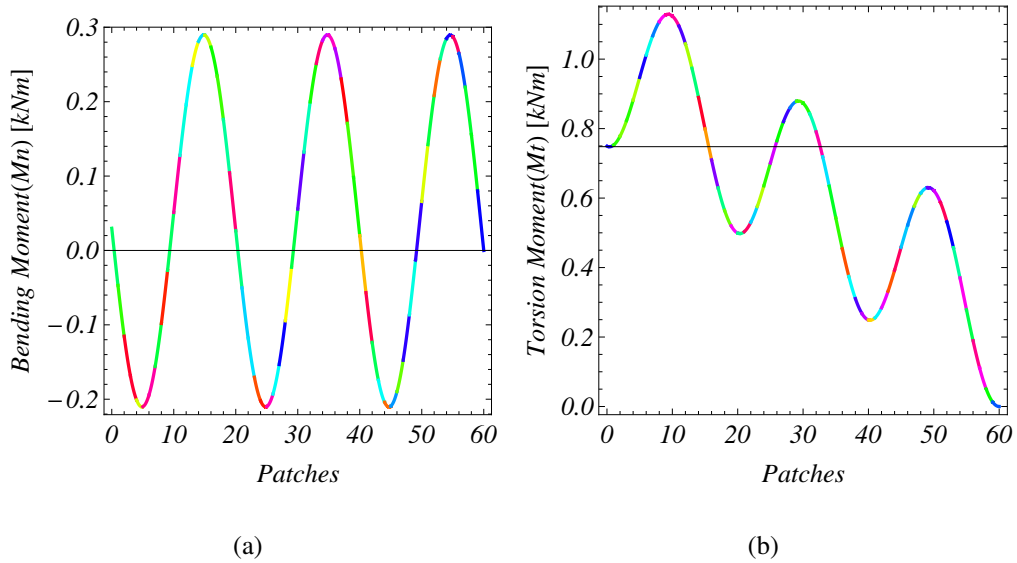


Figure 11: Stress resultant for the helix; 11(a) Bending moment; 11(b) Twisting moment.

6.6 Multipatch assembly of 3D space rods

In this section it is considered a case of assembly of Kirchhoff-Love rods. The rods are defined on a prescribed surface, considering a double family of curves on it. The normal \hat{n}_0 coincides with the normal to the surface, in this sense the unit frame of directors is not geodetic for the centroid curve and the initial rod geometry is affected by initial curvatures and torsion.

6.6.1 The hyperboloid grid-surface

We start with an hyperboloid surface, with a square basis of side 1 [m]- One vertex is raised by 0.25 [m] with respect to the others. Two families of non-geodetic curves on this surface are considered, with uniform relative distance along the X-direction and Y-direction. The centroid curves of the rods are defined by straight lines, while the normal vector \hat{n}_0 is the the normal of surface, so that the intrinsic triads the rods is affected by an initial torsion. The sections dimensions are respectively $h_n = 0.1$, [m] and $h_\nu = 0.05$, [m] along the n-direction and the ν -direction, the Young's modulus considered is $E = 1.999 * 10^{-8}$, [kN/m] and a point force $F = \{0, 0, -1\}$, [kN] is applied on the highest vertex. The deformed shape of the grid is superposed to the original configuration in figure 12.

The examples demonstrates the ability of the method to treat complex rod assemblies, The re-parametrization of the dof's allows to treat these cases without special elements or without adding new constraint equations to the problem. In figures 13 are reported the bending moments and the twisting moment along an edge beam. The discontinuities in the joints are correctly accounted for using the geometric intrinsic continuity proposed.

7 CONCLUSIONS

The main findings of the paper are as follows:

- a model for Kirchhoff-Love rods has been presented, that employs as degrees of freedom the position vector of the point of the rod axis and the torsional rotation around the current tangent;

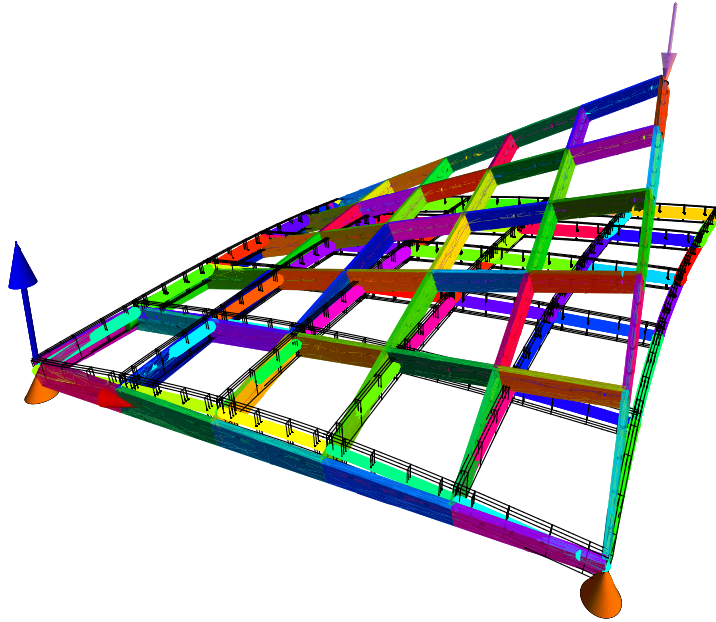


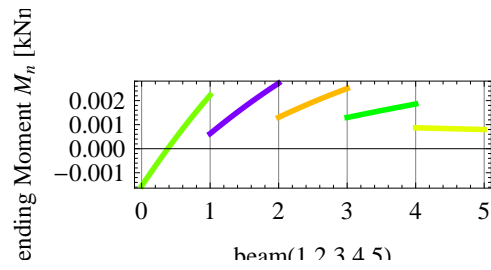
Figure 12: Initial and deformed configurations of the hyperboloid Kirchhoff-Love grid.

- the model has been implemented in a numerical scheme based on B-splines interpolation;
- two strategies have been compared, one that employs a single patch for the whole rod, and the other that employs a multiple patch discretization with G^1 geometric continuity at the joints; a change of basis for the degrees of freedom has been used for enforcing the G^1 continuity;
- convergence analyses have been carried out on a number of examples, which have shown that with single patch interpolation the rate of convergence equals the degree p of the B-splines, while with multiple patches the rate of convergence at most reaches $p - 1$;
- results on membrane locking have been presented, showing that locking is present, but reduces with increasing degree of the spines. No difference is observed between single and multi-patch interpolations.

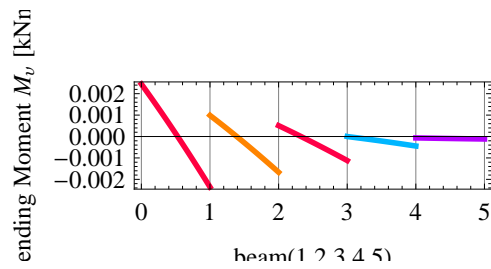
REFERENCES

- [1] A. Goriely, M. Nizette and M. Tabor. On the dynamic of elastic strips. *J. Nonlinear Sci.*, **11**, 3–45, 2001.
- [2] J. Langer and D.A. Singer. Lagrangian aspects of the kirchhoff elastic rod. *SIAM REVIEW*, **38**, 605–618, 1995.
- [3] S. S. Antman. *Nonlinear problem of elasticity*. Springer-Verlag, New York, 1995.

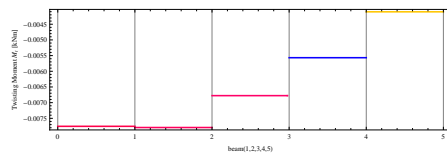
- [4] J. C. Simo and L. Vu-Quoc. A three dimensional finite strain rod model. part ii: computational aspect. *Comput. Methods Appl. Mech. Engrg.*, **58**, 79–116, 1986.
- [5] M. A. Crisfield. A consistent co-rotational formulation for non-linear, three-dimensional, beam elements. *Comput. Methods Appl. Mech. Engrg.*, **81**, 131–150, 1990.
- [6] G. Becker and L. Noels. A fracture framework for euler-bernouilli beams based on a full discontinuous galerkin formulation/extrinsic cohesive law combination. *Int. J. Numer. Meth. Engrg.*, **85**, 1227–1251, 2011.
- [7] J.C. Simo. A three dimensional finite strain rod model. part ii, computational aspects. *Compt. Methods Appl. Mech. Engrg.*, **58**, 79–116, 1986.
- [8] C. Gontier and C. Vollmer. A large displacement analysis of beam using a cad geometric definition. *Computer and Structure*, **57**(6), 981–989, 1995.
- [9] R. Echter and M. Bischoff. Numerical efficiency, locking and unlocking of nurbs finite elements. *Comput. Methods Appl. Mech. Engrg.*, **199**, 374–382, 2010.
- [10] M. Cuomo L. Greco. B-spline interpolation of kirchho-love space rods. .
- [11] F. Armero and J. Valverde. Invariant hermitian finite elements for thin kirchhoff rods. i: The linear plane case. *Comput. Methods Appl. Mech. Engrg.*, **213-216**, 427–457, 2012.
- [12] F. Armero and J. Valverde. Invariant hermitian finite elements for thin kirchhoff rods. ii: The linear three-dimensional case. *Comput. Methods Appl. Mech. Engrg.*, **213-216**, 458–485, 2012.
- [13] L. Piegl and W. Tiller. *The NURBS Book*. Springer-Verlag, New York, 2 edition, 1995.
- [14] R.H McNeal and R.L. Harder. A proposed standard set of ptoblems to test finite elements accuracy. *FE Analysis and Design*, **1**, 3–20, 1985.



(a)



(b)



(c)

Figure 13: Stress resultant for the first beam line of the hypar; 13(a) Bending moment M_n ; 13(b) Bending moment M_b ; 13(c) Twisting moment.